HiSST: 3rd International Conference on
High-Speed Vehicle Science Technology
14 -19 April 2024, Busan, Korea

Numerical Performance Assessment of Vitiated Air Heater for DCSC Test Facility by 3D LES

Bu-Kyeng Sung[1], Seung-Min Jeong[2], Min-Su Kim[3], Jeong-Yeol Choi[4]

Abstract

To better understand the combustion characteristics of a vitiated air heater (VAH) in a direct-connect supersonic combustor, we conducted a Large Eddy Simulation (LES) using the 'reactingFoam' solver from OpenFOAM. The VAH comprised a GH_2/GO_2 single coaxial shear injector for heat addition, surrounded by 24 air injectors for air supply and film cooling. The combustor wall could be thermally insulated by introducing coolant injection and additionally, the turbulent motion could be promoted in the combustion zone. The combustion process completed within the initial one-third length of the combustor, results in a uniform total temperature distribution that aligns with the intended adiabatic flame temperature.

Keywords: Direct-Connect Scramjet Combustor(DCSC), Test Facility, Vitiated Air Heater, Film Cooling,

1. Introduction

In the development phase of hypersonic flight vehicles, ground test facilities are crucial. These facilities are constructed in various ways, with operation times ranging from milliseconds to continuous operation. However, the cost of building an experimental facility is proportional to its operable time and the scale of the experiment. During scramjet combustion experiments, combustion instability in the supersonic combustion flow field has been discovered and is being analyzed through both experimental and numerical methods. This low-frequency supersonic combustion instability occurs at a few hundred Hz. The pulse-type test facilities, which operate for approximately 1 ms, are not suitable for capturing and analyzing this periodic instability. The blowdown type test facilities, which have operation times in the order of seconds, offer three options for air heaters that vitiate air with combustion products, air dissociation, and particulates, respectively. Among these options, for laboratory-scale combustion experiments, the combustion-type vitiated air heater using a rocket combustor and supersonic nozzle is the simplest and cheapest option.

The design of the combustor for the vitiated air heater is based on the well-known CFD validation case PSU-RCM1 of Pennsylvania State University [1,2]. Our research group was able to design the Vitiated Air Heater by incorporating some ideas into the PSU-RCM1 combustor, leveraging our experience in simulation and analysis of the rocket combustor [3-8]. To mimic and supply high-enthalpy supersonic flow into the scramjet isolator, the oxygen mass fraction of the combustion product of the vitiated air heater must match the species composition of the standard atmosphere. Therefore, additional air injectors are introduced on the base model combustor, which utilizes a GH_2/GO_2 shear coaxial injector.

[1] *Department of Aerospace Engineering, Pusan National University, Busan 46241, Korea, tjdqnrud91@pusan.ac.kr*
[2] *Department of Aerospace Engineering, Pusan National University, Busan 46241, Korea, smjeong@kari.re.kr*
[3] *Department of Aerospace Engineering, Pusan National University, Busan 46241, Korea, rotation17@naver.com*
[4] *Department of Aerospace Engineering, Pusan National University, Busan 46241, Korea, aerochoi@pusan.ac.kr*

From the VAH design perspective, the additional air injectors operate as the main air supply, while the GH_2/GO_2 shear coaxial injector adds heat to the main air stream.

During the design process, it was taken into account that injecting the fluid tangentially into the combustor wall through slots or holes could provide thermal insulation between the flame zone and the wall [9]. This technique not only cools the combustor wall but also enhances turbulent motion in the combustion zone, resulting in a homogeneous combustion product being supplied to the scramjet combustor. Thus, coolant air injection was employed in the design to achieve these benefits. The configuration of the designed vitiated air heater can be seen in Fig. 1 and 2.

Previously, in our group, most of the CFD simulation, including the simulation of the scramjet combustor in Fig. 1 [10,11], was conducted using in-house structured grid CFD codes 'RPL2D' and 'RPL3D' [12-25]. However, the VAH designed in the present paper has quite a complex geometry to build the mesh in a structured grid system. Therefore, the 'reactingFoam' solver in OpenFOAM is employed in this study.

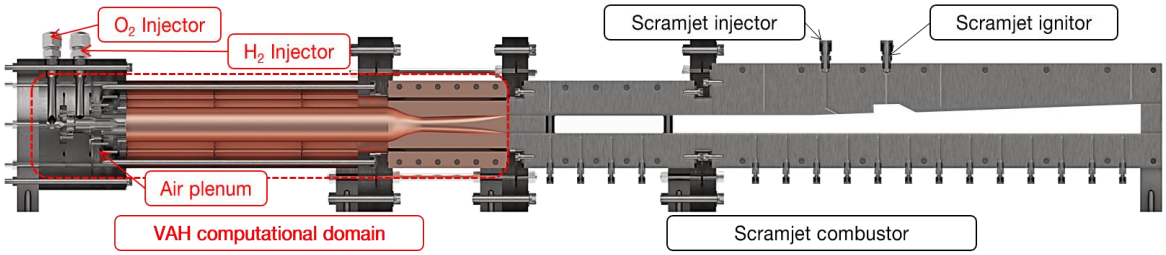

Fig 1. Configuration of Direct-connect Scramjet-test Facility

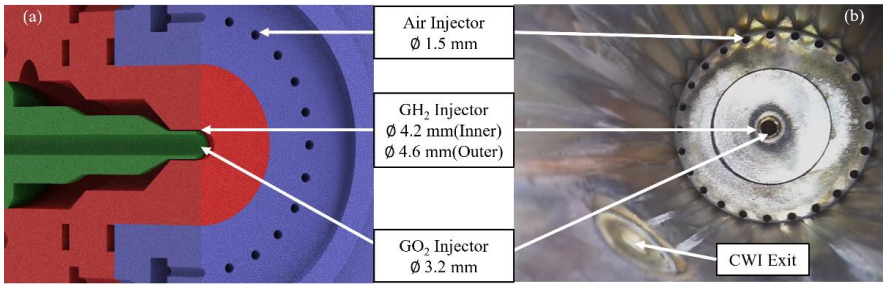

Fig 2. VAH head shear coaxial GH_2/GO_2 injector. (a) CAD model. (b) Experimental model

2. Methodology

The combustor is designed by tracing the operating condition reversely from the supersonic combustor exit to the vitiated air heater to achieve the ideal expansion at the supersonic combustor exit on the ground test. Theoretically, the pressure and temperature at the upstream and downstream of the nozzle were 17.3248 bar and 1,578 K and 2.258 bar and 1,000 K, respectively, with the Mach number of 2 at the nozzle exit. The reactant species composition and temperature upstream of the nozzle were calculated using Eq. 1-3. Eq. 1 is formulated to determine the composition of a and b, wherein the oxygen composition of the combusted gas flowing into the supersonic combustor is the same as that of the standard atmosphere. In Eq. 2, the relationship between a and b, 1/2 implies the oxygen injected for the stoichiometric conditions while 1/3.76 is for the compensation of combusted oxygen. The hydrogen and oxygen from the coaxial injector are supplied into the combustor in a certain proportional relation. Therefore, compositions a and b are determined by Eq. 3 to satisfy the desired adiabatic flame temperature. The mass flow rate of the hydrogen, oxygen, and air injector is calculated as 5.683, 69.043, and 293.525 g/s, respectively. From the measurement of the experiment, the mass flow rate was measured as 4.973, 65.439, and 292.275 g/s, thus the equivalence ratio is changed slightly. In the simulation, the experimentally measured mass flow rate is used.

reactingFoam solver of the OpenFOAM is employed in this study. The one-equation eddy viscosity Large Eddy Simulation (LES) turbulence model, and the Partially Stirred Reactor (PaSR) turbulence-chemistry interaction model along with a detailed hydrogen/air chemical kinetics mechanism developed by Jachimowski [26] are employed for turbulence and combustion model, respectively. From previous studies of our group, we have tested the performance of the chemical kinetics mechanisms. The chemical kinetics mechanism developed by Jachimowski [26] was selected based on the previous studies of our group [27-37]. The Crank Nicolson and MUSCL second-order discretization of both spatial and temporal terms is used, respectively. The computational domain contained a total of 13.4 million cells, and a tetrahedral-type grid was used due to the complex geometry adjacent to the coolant air injectors.

The quality of the calculation was ensured by analyzing the pressure history and turbulent kinetic energy spectrum in the combustor, as shown in Fig. 3 to 5. The pressure history of the simulation initially showed large amplitude fluctuation due to the shock wave caused by the unrealistic initial condition. To properly develop the injector flow, the pressure inside the combustor was initialized with half the magnitude of that of the injector upstream. The flame was initiated by setting the initial temperature of the combustor to 1,200 K. After the unsteady behavior, the pressure reached its steady state at around 10 milliseconds and showed good agreement with the steady pressure level of the experiment. The turbulent kinetic energy spectrum also showed agreement with Kolmogorov's -5/3 power law throughout the combustor (the locations x= -0.342, -0.3, 0.0 corresponds to the injector face, middle of the combustion zone, and the nozzle throat, respectively).

$$O_2 + 3.76\mathrm{N}_2 + aH_2 + bO_2 \rightarrow O_2 + 3.76\mathrm{N}_2 + aH_2O + \left(b - \frac{a}{2}\right)\mathrm{O}_2 \qquad (1)$$

$$b = \left(\frac{1}{2} + \frac{1}{3.76}\right)a \qquad (2)$$

$$\sum N_i\left[\bar{h}^0_{f,i} - \bar{c}_{p,i}(T_{ad} - T)\right] = 0 \qquad (3)$$

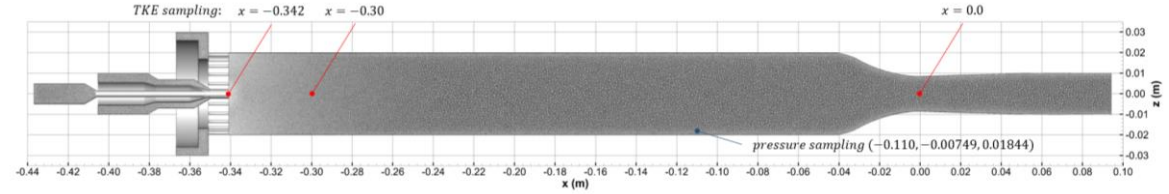

Fig 3. Grid structure and its sampling points.

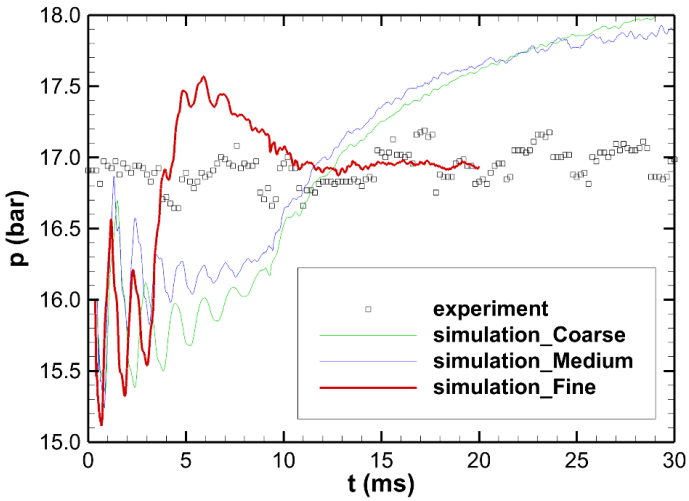

Fig 4. Temporal pressure development of simulation (line) and steady state pressure history of experiment (symbol) in the combustor.

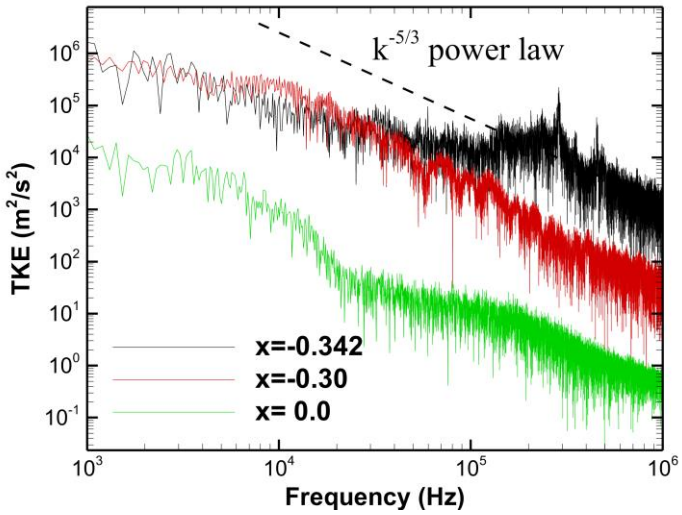

Fig 5. Resolved kinetic energy spectrum at the coaxial injector outlet (black color), middle of the combustion zone (red color), and the nozzle throat (green color).

3. Result and discussion

3.1. Flow and combustion characteristics of vitiated air heater

In Fig. 6, the 3D contour of temperature, OH mass fraction, and the Q-criterion are shown to analyze the overall characteristics of the vitiated air heater. In the temperature distribution, the high-temperature zone is only distributed right downstream of the injector head. The OH mass fraction distribution which can be seen in xz-plane slices in the second picture is also confined to roughly one-third of the combustor length. The recirculation zone formed (negative u-velocity) is noted by the green contour line. By juxtapositioning the contour line of the negative u-velocity contour line and the OH mass fraction distribution, we can see that at the contact surface of the recirculation zone and the coolant air injection, a small amount of the OH is generated. The unburnt hydrogen is entrained into the recirculation zone without leaving the combustion zone at an unburnt state, thus almost complete combustion is achieved. Thus, we came to know that the introduction of coolant injection tangential to the wall changes the combustion and flow characteristics completely.

In the Q-criterion contour [38], in Fig. 6, it can be seen that turbulent eddies are present at the injector head. The combustion zone is crowded by turbulent eddies. It is clear that the turbulent eddy motion developed by the coolant injection and the induced recirculation zone contribute to fuel-air mixing and better combustion. After the high-temperature zone, the streamline becomes almost straight in the remaining combustor. Also in the Q-criterion distribution, the turbulent eddies are barely observed after the combustion zone.

In Fig. 7, the scatter plots of OH mass fraction as a function of mixture fraction are shown to take a closer look into the flame structure. The temperature peak is revealed at two OH mass fraction values, at 0.1 and 0.05. In the scatter plot colored by the u velocity, it can be understood that the first combustion zone is formed along the GH_2/GO_2 flow with higher velocity. In the scatter plot of the Takeno flame Index (F.I.) [39], it can be known that the first combustion zone along the coaxial injector flow is held in diffusive mode except for the mixture fraction above 0.3. The premixed combustion zone is formed right downstream of the coaxial shear injector at a low temperature. It can be understood that hydrogen and oxygen are mixed before they are heated enough to be ignited downstream of the coaxial shear injector at a low temperature. Due to the intense heat release of the premixed combustion zone, the following combustion is held in diffusive mode. After this diffusive combustion, the leftover fuel species flow into the recirculation zone. The second combustion zone is formed at the lower mixture fraction and OH mass fraction showing the negative u velocity which means the recirculation zone, therefore showing the second temperature peak. In the recirculation zone, the hydrogen and OH are

completely consumed still in the diffusive mode. In the scatter plot of the heat release rate, it can be known that the heat is released intensely along the coaxial injector flow region while the heat release in the recirculation zone is comparatively small.

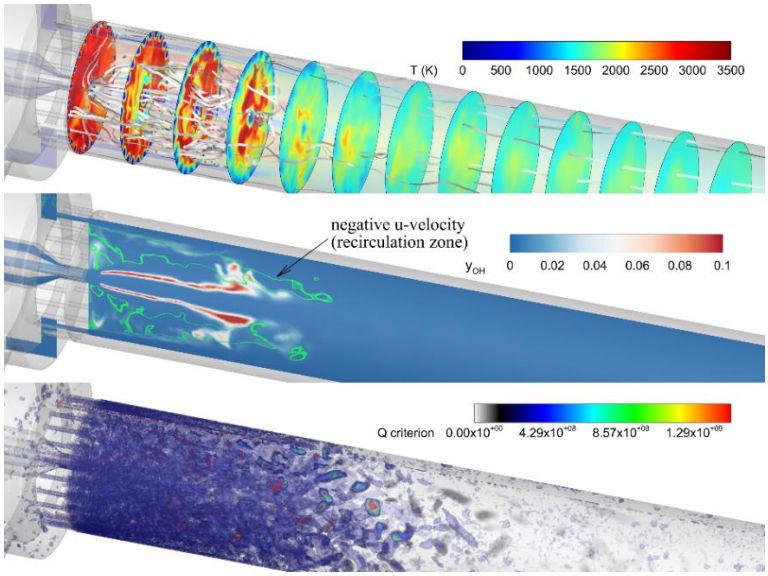

Fig 6. Temperature, OH, and Q distribution of vitiated air heater. The longitudinal slice shows the OH mass fraction distribution. The green contour line shows the negative u-velocity contour lines which shows the recirculation region. The third picture shows the iso-surfaces of the Q-criterion.

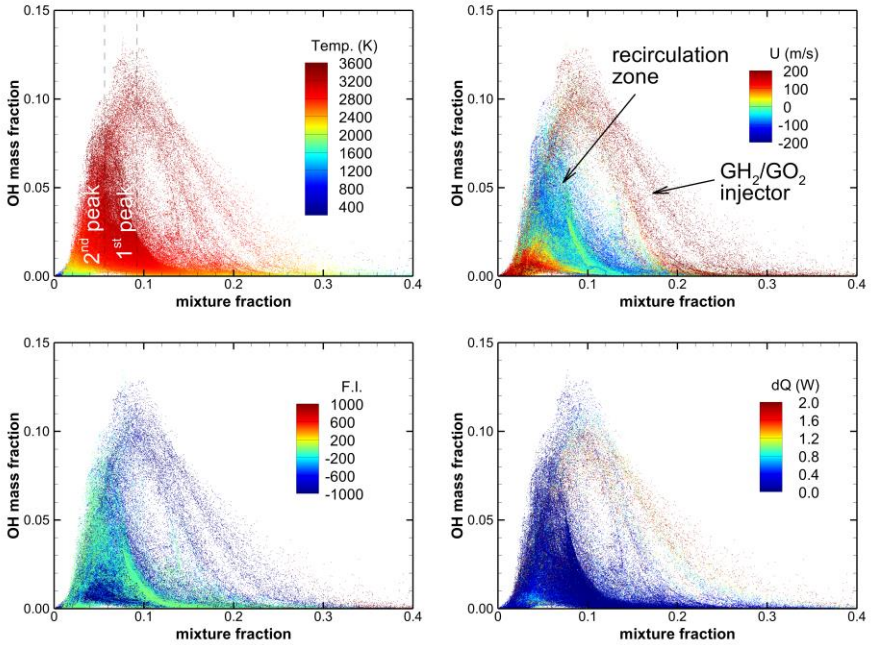

Fig 7. Scatter plots of OH mass fraction as function of mixture fraction colored by the temperature, u velocity, Takeno flame index, F.I., and heat release rate, dQ.

In Fig. 8, the overall combustion and flow characteristics of vitiated air heater are shown. The time-averaged hydrogen and oxygen mass fraction and u-velocity contour lines are superimposed to identify

the overall combustion field characteristics. As mentioned earlier, due to the negative velocity of the recirculation zone, a portion of the coolant air and unburnt hydrogen lose their momentum. This leads the air and hydrogen entrained into the recirculation zone. Therefore, due to the coolant injection, the injected hydrogen is confined and completely consumed in this region.

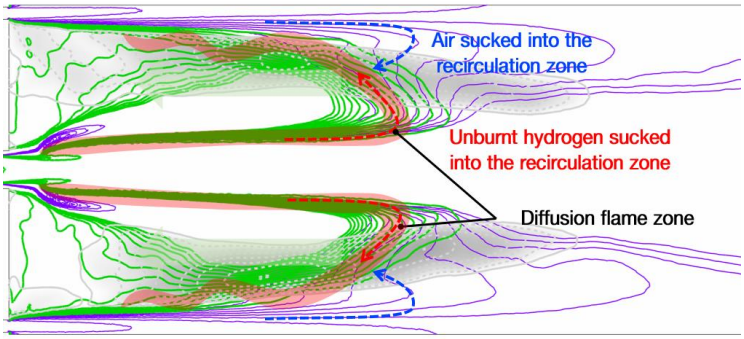

Fig 8. Time-averaged flow feature of vitiated air heater. Green line indicates the hydrogen mass fraction distribution from 0 to 0.1. Purple line indicates the Oxygen mass fraction distribution from 0 to 0.25. Gray line indicates the negative u-velocity from -200 to 0 (m/s), i.e. recirculation zone.

3.2. Nozzle performance evaluation and the comparison with the experiment

In this section, the supersonic nozzle connecting the vitiated air heater to the supersonic combustor is analyzed. The computational grid at the nozzle section was kept minimized to focus on the combustion phenomena of the vitiated air heater. The insufficient number of grids in the nozzle wall resulted in the boundary layer being thicker than the physical thickness.

Therefore, the nozzle performance of the current numerical simulation is compared with the experimental data [40,41] and the nozzle design study [42] to analyze the nozzle performance. In Fig. 9, the species mass fraction, temperature, and pressure distribution at the nozzle exit are compared. The nitrogen distribution shows fairly good agreement with the targeted mass fraction of the product. Due to the decreased overall equivalence ratio of the experiment compared to the theoretical calculation, oxygen is less consumed, and therefore water vapor is less produced compared with the targeted product mass fraction. As mentioned in chapter 2, the resulting species mass fraction distribution can be understood. It can be found that the air injected by the cooling port shows a small gap between the theoretical and the experimental value whereas the hydrogen and oxygen decreased largely.

In Table 1, the temperature and pressure calculated by the theoretical relation and simulation are shown. Due to the thickly developed boundary layer, the temperature and pressure are not properly expanded. Comparing the nozzle inlet and the exit condition, it can be found that the temperature and pressure ratio corresponds to the Mach number of about 1.8. In Fig. 10, the Schlieren photograph of Mach number evaluation is shown. In the experiment, the nozzle Mach number evaluation is conducted under different total pressure conditions. As a result of the experiment, it has been shown that the nozzle operates in the Mach number of 2.04±0.04 regardless of the upstream condition [40,41]. Also, a separate simulation including the effect of combustion [43] was conducted to compare the result with the experiment by following the design process of reference [42]. It has been found that the temperature and pressure at the nozzle exit exhibit a uniform distribution with the Mach number of 2.01. The temperature and pressure distribution at the nozzle exit are compared in Fig. 9 with dashed lines. Through the nozzle exit Mach number achieved from the experiment [40,41] and the nozzle simulation [42,43], it becomes obvious that the pressure and temperature ratio will be very similar to the theoretical value. Thus, if we estimate the exit condition, it agrees fairly well with the design condition. In Fig. 11, the 2D-like shock structure is clearly observed in the single cavity combustor which can be understood as the evidence of the generation of the uniform flow of the shape transition

nozzle [40,41]. Through the confirmation of the operability of the designed VAH, the scramjet experiment [44] is now being conducted with confidence.

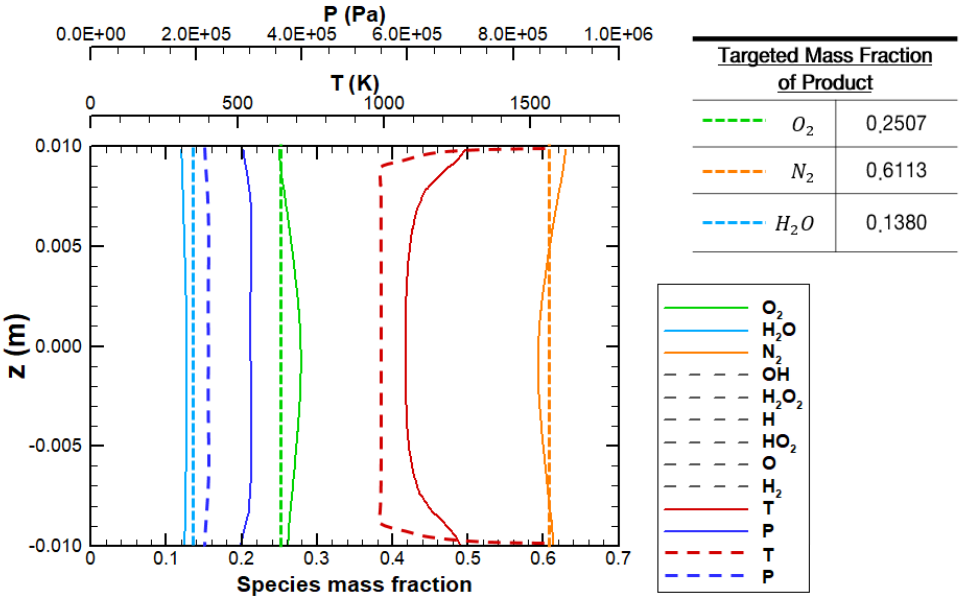

Fig 9. Species, Temperature, and pressure distribution at the nozzle exit. Dashed lines for species have very small mass fractions close to zero. The Solid lines for temperature and pressure are the value of current simulation, and dashed lines are a reference value of the nozzle design study of reference [43].

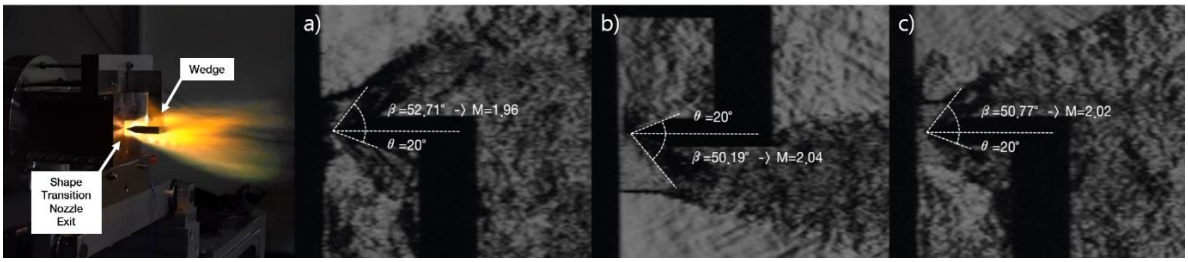

Fig 10. Exit Mach number evaluation by Schlieren photograph of current vitiated air heater using $\boldsymbol{\theta - \beta - M}$ relation at the nozzle exit [40,41].

Table 1. The theoretical and numerical value of operating condition of supersonic nozzle. Estimated range of temperature and pressure based on the Mach number measured from the experiment.

	Temperature (K)	Pressure (bar)	Temperature ratio	Pressure ratio
Theoretical nozzle inlet condition	1,578	17.27	1.58	7.65
Theoretical nozzle exit condition	1,000	2.258		
Present nozzle inlet condition	1,577	16.94	~1.47	~5.60
Present nozzle exit condition	1,073	3.031		
Estimated exit condition	**~ 998.1**	**~ 2.21**		

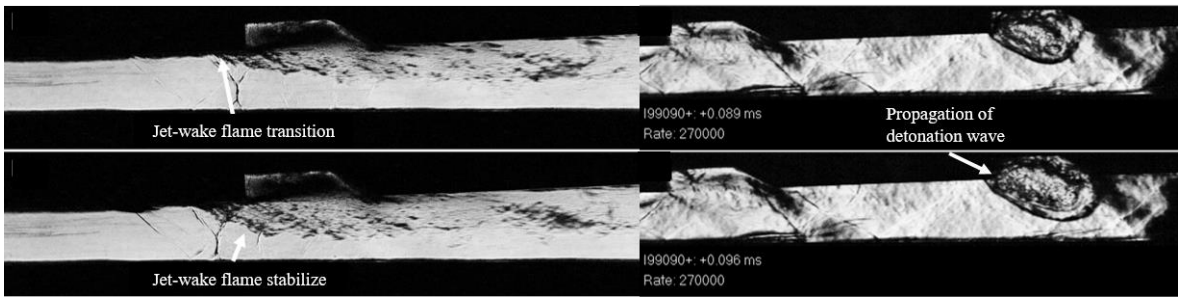

Fig 11. Schlieren image of the scramjet experiment. (left) single and (right) tandem cavity scramjet experiment with flow excitation by the pulse detonation engine [44]

4. Conclusion

The Large Eddy Simulation (LES) is conducted using the reactingFoam solver in OpenFOAM to comprehensively analyze the combusting flow field and operational performance of a compact rocket-type vitiated air heater for direct-connect supersonic combustion experiments. This vitiated air heater design features a single coaxial shear injector and 24 coolant air injectors.

The introduction of coolant injection alongside the coaxial shear injector leads to the formation of a recirculation zone between the coolant air and the core GH_2/GO_2 flow of the coaxial injector. Our design entrains unburnt hydrogen into the recirculation zone, ensuring complete combustion within a shorter length of the combustor. This combustion process results in uniform temperature distribution and achieves the intended adiabatic flame temperature. The coolant injection not only insulates the combustor wall from high-temperature regions but also enhances turbulent eddy motion within the combustion zone, promoting efficient combustion.

The exit of the supersonic nozzle demonstrates fairly good agreement in nitrogen distribution with theoretical predictions. However, due to reduced equivalence ratio, less water vapor is produced, and some oxygen remains unburnt. Nevertheless, the product mass fraction exhibits a suitably uniform distribution. The supersonic nozzle exit conditions were estimated based on experimental Mach number measurements, and the estimated range aligns well with theoretical expectations.

Our study highlights the successful implementation of coolant injection in the vitiated air heater design, leading to enhanced combustion efficiency. The combination of LES simulations and experimental validation provides valuable insights into the performance and characteristics of the proposed design, contributing to the advancement of supersonic combustion technologies.

Acknowledgments

Present work was funded by the Basic Research Program (No. 08-201-501-014) of the Agency for Defense Development (ADD) supported by the Defense Acquisition Program Administration (DAPA) of the Korean Government.

References

1. Pal, S., Marshall, W., Woodward, R., Santoro, R.: Wall heat flux measurements for a uni-element GO_2/GH_2 shear coaxial injector. *Third International Workshop on Rocket Combustion Modeling*, pp. 13-15. (2006)
2. MARSHALL, W., Pal, S., Woodward, R., Santoro, R.: Benchmark wall heat flux data for a GO_2/GH_2 single element combustor. *41st AIAA/ASME/SAE/ASEE Joint Propulsion Conference & Exhibit. (2005)*. https://doi.org/10.2514/6.2005-3572

3. Jeong, S. M., Um, J. R., Choi, J. Y.: Numerical Study of High Resolution Schemes for GH_2/GO_2 Rocket Combustor using Single Shear Coaxial Injector, *J. of the Korean Society of Propulsion Engineers* (2018). https://doi.org/10.6108/KSPE.2018.22.6.072
4. Hwang, W.-S., Han, W., Huh, K. Y., Lee, B. J., Han, H.-S., Sohn, C.H., Choi, J.-Y.: Real-gas-flamelet-model-based numerical simulation and combustion instability analysis of a GH_2/LOX rocket combustor with multiple injectors. *Energies* (*2021),* https://doi.org/10.3390/en14020419
5. Hwang, W.-S., Han, W., Huh, K. Y., Kim, J., B.J., Choi, J.-Y.: Numerical simulation of a GH_2/LOX single injector combustor and the effect of the turbulent Schmidt number. *Energies* (2020), https://doi.org/10.3390/en13246616
6. Park, G., Oh, S., Yoon, Y., Choi, J.-Y.: Characteristics of gas-centered swirl-coaxial injector with liquid flow excitation. *J. Propuls. Power* (2019), https://doi.org/10.2514/1.B36647
7. Natarajan, V., Unnikrishnan, U., Hwang, W.-S., Choi, J.-Y., Yang, V.: Numerical study of two-phase flow dynamics and atomization in an open-type liquid swirl injector. *Int. J. Multiph. Flow* (2021), https://doi.org/10.1016/j.ijmultiphaseflow.2021.103702
8. Natarajan, V., Unnikrishnan, U., Choi, J.-Y., Yang, V.: Flow dynamics of a liquid–liquid bi-swirl injector. *Phys. Fluids* (2024). https://doi.org/10.1063/5.0191490
9. SHINE, S. R., NIDHI, S. Shri.: Review on film cooling of liquid rocket engines. *Propuls. Power Res.* (2018), https://doi.org/10.1016/j.jppr.2018.01.004
10. Jeong, S.-M., Choi, J.-Y.: Combined diagnostic analysis of dynamic combustion characteristics in a scramjet engine. *Energies* (2020), https://doi.org/10.3390/en13154029
11. Jeong, S.-M., Han, H.-S., Sung, B.-K., Kim, W., Choi, J.-Y.: Reactive Flow Dynamics of Low-Frequency Instability in a Scramjet Combustor. *Aerospace* (2023). https://doi.org/10.3390/aerospace10110932
12. Shin, J.-R., Cho, D.-R., Won, S.-H., Choi, J.-Y.: Hybrid RANS/LES study of base-bleed flows in supersonic mainstream. *15th AIAA International Space Planes and Hypersonic Systems and Technologies Conference,* (2008). https://doi.org/10.2514/6.2008-2588
13. Won, S.-H., Jeung, I.-S., Choi, J.-Y.: Turbulent combustion characteristics in HyShot model combustor with transverse fuel injection. *43rd AIAA/ASME/SAE/ASEE Joint Propulsion Conference*, (2007). https://doi.org/10.2514/6.2007-5427
14. Choi, J.-Y., Ma, F., Yang, V.: Dynamics combustion characteristics in scramjet combustors with transverse fuel injection. *41st AIAA/ASME/SAE/ASEE Joint Propulsion Conference and Exhibit*. (2005). https://doi.org/10.2514/6.2005-4428
15. Choi, J.-Y., Shin, E., Kim, C.-K.: Numerical study of base-bleed projectile with external combustion. *41st AIAA/ASME/SAE/ASEE Joint Propulsion Conference and Exhibit*. (2005). https://doi.org/10.2514/6.2005-4352
16. Choi, J.-Y., Yang, V., Ma, F., Won, S.-H., Jeung, I.-S.: Detached Eddy simulation of combustion dynamics in scramjet combustors. *43rd AIAA/ASME/SAE/ASEE Joint Propulsion Conference* (2007). https://doi.org/10.2514/6.2007-5027
17. Won, S.-H., Jeung, I.-S., Choi, J.-Y.: DES study of transverse jet injection into supersonic cross Flows. *44th AIAA Aerospace Sciences Meeting* (2006). https://doi.org/10.2514/6.2006-1227
18. Won, S.-H., Jeung, I.-S., Choi, J.-Y.: DES investigation of the ignition of hydrogen transverse jet into high enthalpy supersonic crossflow. *47th AIAA Aerospace Sciences Meeting including the New Horizons Forum and Aerospace Exposition,* (2009). https://doi.org/10.2514/6.2009-1557
19. Choi, J.-Y., Yang, V., Fuhua, M., Won, S.-H.: Jeung, I.-S. DES Modeling of Supersonic Combustion in Scramjet Combustors. *AIAA/ASME/SAE/ASEE 42nd Joint Propulsion Conference* (2006). https://doi.org/10.2514/6.2006-5097

20. Won, S.-H., Jeung, I.-S., Shin, J.-R., Cho, D.-R., Choi, J.-Y.: Three-dimensional dynamic characteristics of transverse fuel injection into a supersonic cross flow. *15th AIAA International Space Planes and Hypersonic Systems and Technologies Conference* (2008). https://doi.org/10.2514/6.2008-2515
21. Kim, J., Jeong, S.–M., Kim, W.D., Choi, J.–Y., Hwang, Y.: Numerical analysis of internal flow thermal environment in an accelerating high–speed vehicle. *Aerosp. Sci. Technol.* (2024). https://doi.org/10.1016/j.ast.2024.108889
22. Choi, J.-Y., Noh, J., Byun, J.-R., Lim, J. S., Togai, K., Yang, V.: Numerical investigation of combustion/shock-train interactions in a dual-mode scramjet engine. *17th AIAA International Space Planes and Hypersonic Systems and Technologies Conference*, (2011). https://doi.org/10.2514/6.2011-2395
23. Vyasaprasath, K., Oh, S., Kim, K.-S., Choi, J.-Y.: Numerical studies of supersonic planar mixing and turbulent combustion using a detached eddy simulation (DES) model. *Int. J. Aeronaut. Space Sci.* (2015). https://doi.org/10.5139/IJASS.2015.16.4.560
24. Noh, J., Choi, J. Y., & Yang, V.: Numerical Simulation of Ethylene Fueled Scramjet Combustor with Air Throttling, Part 1: Auto-Ignition. *Journal of Propulsion and Energy* (2020). https://doi.org/10.6108/JPNE.2020.1.1.032
25. Choi, J. Y., Noh, J., Jeong, S. M., Kim, J. E., Yang, V.: Numerical Simulation of Ethylene Fueled Scramjet Combustor with Air Throttling, Part2: Transient Details. *Journal of Propulsion and Energy* (2021). https://doi.org/10.6108/JPNE.2021.2.1.044
26. Jachimowski, C.J.: An analytical study of the hydrogen-air reaction mechanism with application to scramjet combustion. Report No. NASA-TP-2791, NASA Langley Research Center, VA, USA. (1988).
27. Kim, S.D., Lee, B.J., Lee, H.J. Jeung, I.-S., Choi, J.-Y.: Realization of contact resolving approximate Riemann solvers for strong shock and expansion flows. *Int. J. Numer. Methods Fluids* (2020). https://doi.org/10.1002/fld.2057
28. Kim, S.-L., Choi, J.-Y., Jeung, I.-S., Park, Y.-H.: Application of approximate chemical Jacobians for constant volume reaction and shock-induced combustion. *Appl. Numer. Math.* (2001). https://doi.org/10.1016/S0168-9274(01)00054-X
29. Kim, S.-L., Jeung, I.-S., Choi, J.-Y., Park, Y.-H.: Approximate Jacobian methods for efficient calculation of reactive flows. *36th AIAA/ASME/SAE/ASEE Joint Propulsion Conference and Exhibit* (2000). https://doi.org/10.2514/6.2000-3384
30. Pavalavanni, P.K., Sohn, C.H., Lee, B.J., Choi, J.-Y.: Revisiting unsteady shock-induced combustion with modern analysis techniques. *Proc. Combust. Inst.* (2019). https://doi.org/10.1016/j.proci.2018.07.094
31. Choi, J.-Y., Jeung, I.-S., Yoon, Y.: Unsteady-state simulation of model ram accelerator in expansion tube. *AIAA J.* (1999). https://doi.org/10.2514/2.770
32. Choi, J.-Y., Jeung, I.-S., Yoon, Y.: Validation of CFD algorithms for unsteady shock-induced combustion. *34th AIAA/ASME/SAE/ASEE Joint Propulsion Conference and Exhibit* (1998). https://doi.org/10.2514/6.1998-3217
33. Choi, J.-Y., Jeung, I.-S., Yoon, Y.: Scaling effect of the combustion induced by shock-wave boundary-layer interaction in premixed gas. *Symp. Combust. Proc.* (1998). https://doi.org/10.1016/S0082-0784(98)80067-2
34. Pavalavanni, P.K., Kim, K.-S., Oh, S., Choi, J.-Y.: Numerical comparison of hydrogen-air reaction mechanisms for unsteady shock-induced combustion applications. *J. Mech. Sci. Tech.* (2015). https://doi.org/10.1007/s12206-015-0202-2
35. Pavalavanni, P.K., Jo, M.-S., Kim, J.-E., Choi, J.-Y.: Numerical Study of Unstable Shock-Induced Combustion with Different Chemical Kinetics and Investigation of the Instability Using Modal Decomposition Technique. *Aerospace* (2023). https://doi.org/10.3390/aerospace10030292

36. Choi, J.-Y., Jeung, I.-S., Yoon, Y.: Transient simulation of superdetonative mode initiation process in scram-accelerator. *Symp. Combust. Proc.* (1996). https://doi.org/10.1016/S0082-0784(96)80138-X

37. Pavalavanni, P.K., Kim, J.-E., Jo, M.-S., Choi, J.-Y.: Numerical Investigation of the Detonation Cell Bifurcation with Decomposition Technique. *Aerospace* (2023). https://doi.org/10.3390/aerospace10030318

38. Jeong, J., Hussain, F.: On the identification of a vortex. *J. Fluid Mech.* (1995). https://doi.org/10.1017/S0022112095000462

39. Yamashita, H., Shimada, M., Takeno, T.: A numerical study on flame stability at the transition point of jet diffusion flames. *Symp. Combust. Proc.* (1996). https://doi.org/10.1016/S0082-0784(96)80196-2

40. Lee, J.-H., Lee, E.-S., Han, H.-S., Kim, M.-S., Choi, J.-Y.: A Study on a Vitiated Air Heater for a Direct-Connect Scramjet Combustor and Preliminary Test on the Scramjet Combustor Ignition. *Aerospace* (2023). https://doi.org/10.3390/aerospace10050415

41. Lee, E.-S., Han, H.-S., Lee, J.-H., Choi, J.-Y.: A Study on the Flow Conditions of the Combustion Air Heater Outlet for the Supersonic Combustion Experiment. *J. of the Korean Society of Propulsion Engineers* (2022), https://doi.org/10.6108/KSPE.2022.26.1.088

42. Sung, B.-K., Choi, J.-Y. Choi.: Design of a Mach 2 shape transition nozzle for lab-scale direct-connect supersonic combustor. *Aerosp. Sci. Technol.* (2021), https://doi.org/10.1016/j.ast.2021.106906

43. Sung, B.-K., Jeong, S.-M., Choi, J.-Y.: Direct-connect Supersonic Nozzle Design Considering the Effect of Combustion," *Aerosp. Sci. Technol.* (2023), https://doi.org/10.1016/j.ast.2022.108094

44. Kim, M.-S., Koo, I.-H., Lee, K.-H., Lee, E.-S., Han, H.-S., Jeong, S.-M., Kim, H., Choi, J.-Y.: Experimental Study on the Ignition Characteristics of Scramjet Combustor with Tandem Cavities Using Micro-Pulse Detonation Engine. *Aerospace* (2023), https://doi.org/10.3390/aerospace10080706

